Remote Sensing of Environment 115 (2011) 180–186

Contents lists available at ScienceDirect

Remote Sensing of Environment

journal homepage: www.elsevier.com/locate/rse

Characterization of MODIS-derived euphotic zone depth: Results for the China Sea

Shaoling Shang [a,b,*], Zhongping Lee [c], Guomei Wei [a]

[a] State Key Laboratory of Marine Environmental Science, Xiamen University, Xiamen 361005, China
[b] Key Laboratory of Underwater Acoustic Communication and Marine Information Technology (Xiamen University), Ministry of Education of China, Xiamen 361005, China
[c] Geosystems Research Institute, Mississippi State University, MS 39529, USA

ARTICLE INFO

Article history:
Received 4 June 2010
Received in revised form 4 August 2010
Accepted 24 August 2010

Keywords:
MODIS
Remote sensing
China Sea
Euphotic zone depth
Chlorophyll-a

ABSTRACT

Euphotic zone depth (Z_{eu}) products from ocean color measurements are now produced from MODIS ocean color measurements, one of which is based on inherent optical properties (IOP-approach) and the other is based on chlorophyll-a concentration (Chl-approach). For the first time, the quality of these satellite Z_{eu} products is assessed with extensive field-measured Z_{eu} (in the China Sea), where 78% of the measurements were made on the continental shelf (≤200 m). For the data with matching location and time window, we have found that the overall average difference (ε) between satellite and *in situ* Z_{eu} is 21.8% (n = 218, Z_{eu} ranges from 4 to 93 m) with a root mean square error in log scale (RMSE) of 0.118 by the IOP-approach, while it is 49.9% (RMSE = 0.205) by the Chl-approach. These results suggest that 1) MODIS Z_{eu} products for waters in the China Sea are robust, even in shelf waters; and 2) Z_{eu} produced with IOPs are more reliable than those produced with empirically derived Chl. Spatial and seasonal variations of Z_{eu} in the China Sea are briefly described with Z_{eu} products generated by the IOP-approach. These results will facilitate further research on carbon cycling and environmental changes on both local and global scales.

1. Introduction

Most marine phytoplankton photosynthesize in the euphotic zone (Kirk, 1994). Although the disphotic zone has recently attracted increasing attention (Buesseler et al., 2007), the euphotic zone is nevertheless the most important zone in the context of both ecosystem dynamics (Platt & Sathyendranath, 1988) and in air–sea interaction through transfer of either heat (Sathyendranath et al., 1991) or gases, especially with regards to green house gases such as carbon dioxide (CO_2) (Takahashi et al., 2002). In practice, the euphotic zone depth (Z_{eu}) is defined as the depth at which the PAR (photosynthetic available radiation) value is 1% of the surface value (Kirk, 1994). The value of Z_{eu} is an important input parameter for many models that estimate basin-scale primary production (Behrenfeld & Falkowski, 1997a,b). Both Secchi disk depth (Preisendorfer, 1986; Tyler, 1968) and Z_{eu} measure water clarity, but Z_{eu} can be measured objectively with advanced electro-optical instruments. Because Z_{eu} is a cumulative measure of biogeochemical properties in the upper-water column, changes in the Z_{eu} depict environmental patterns that might be associated with climate. Thus it is not surprising to see that Z_{eu} is included as a standard ocean color product in the Global Change Observation Mission (Japan, http://suzaku.eorc.jaxa.jp/GCOM_C) and that Z_{eu} products for the global ocean are now derived from MODIS (Moderate Resolution Imaging Spectroradiometer) measured water-leaving radiance. Numerous studies have been carried out to evaluate the quality of satellite-derived chlorophyll concentration (Chl) and the diffuse attenuation coefficient (Bailey & Werdell, 2006; Darecki & Stramski, 2004; Melin et al., 2007; Zhang et al., 2006). While it is important to know the quality of satellite-derived products before they can be further applied to the study of biogeochemistry and environmental changes, there hasn't been any published independent research (to our knowledge) to evaluate or characterize the quality of MODIS-derived Z_{eu}.

In general, there are two approaches to estimate Z_{eu} from ocean color remote sensing (Lee et al., 2007; Morel et al., 2007). The simple Chl-approach is an empirical method based on Case-1 assumptions (Morel et al., 2007), where Z_{eu} is calculated from concentration of chlorophyll-a (Chl). A different approach (IOP-approach) is centered on waters' inherent optical properties (IOPs) (Lee et al., 2007); Z_{eu} is computed after the absorption and backscattering coefficients at 490 nm are provided. The inputs, either Chl or IOPs, can be obtained from water samples or from the inversion of measured water color (Gordon & Morel, 1983; IOCCG, 2006). Results from both approaches have been tested or validated with ship borne measurements (Lee et al., 2007; Morel et al., 2007), but there hasn't been any test or evaluation of these products when they are derived from satellite data.

In this study, using Z_{eu} data measured in the China Sea over the past six years, we assessed the Z_{eu} products (from both Chl-approach and IOP-approach) derived from MODIS measured ocean color. These measurements were mainly made in the shelf water (≤200 m) to

* Corresponding author. State Key Laboratory of Marine Environmental Science, Xiamen University, Xiamen 361005, China. Tel./fax: +86 592 2184781.
E-mail addresses: slshang@gmail.com, slshang@xmu.edu.cn (S. Shang).

0034-4257/$ – see front matter © 2010 Elsevier Inc. All rights reserved.
doi:10.1016/j.rse.2010.08.016

gauge the quality of satellite products over coastal waters. Finally, we discuss spatial and seasonal variations of Z_{eu} in the China Sea.

2. Data and methods

2.1. In situ Z_{eu} and its uncertainty

A series of field measurements of biological and optical properties were carried out between 2004 and 2009 in different seasons in the China Sea (Fig. 1). Based on equipment availability, the vertical profiles of PAR were measured with a hyperspectral irradiance meter or a broadband PAR sensor, and Z_{eu} values were calculated (detailed below) from the spectrally-integrated PAR profiles. Because Z_{eu} measures a relative difference between PAR(z) (z represents depth from sea surface) and PAR(0), the absolute value that represents PAR has only minor impacts on the value of Z_{eu} (Morel & Gentili, 2004).

2.1.1. Z_{eu} from hyperspectral E_d

In 2007, hyperspectral (350–700 nm, ~3 nm spectral resolution) downwelling irradiance ($E_d(\lambda)$) was measured with a Profiler II (Satlantic, Inc) in the South China Sea (blue symbols in Fig. 1). The Profiler II was lowered into water ~50 m away from an operational ship. E_d profiles were measured in the upper ~150 m and were processed with Satlantic software (Prosoft 7.7.10). Vertical profiles of the total downwelling irradiance in the visible domain Evis(z) were calculated by summing $E_d(\lambda, z)$ from 350 nm to 700 nm for each depth, and then the profiles of Evis(z)/Evis(0) were obtained. Z_{eu} was derived at the depth where Evis(z)/Evis(0) = 1% (Lee et al., 2005, 2007).

2.1.2. Z_{eu} from PAR sensor

For the cruises during the period of 2004–2009, PAR (400–700 nm) was measured with a PAR sensor (PAR_{Bios}, Biospherical

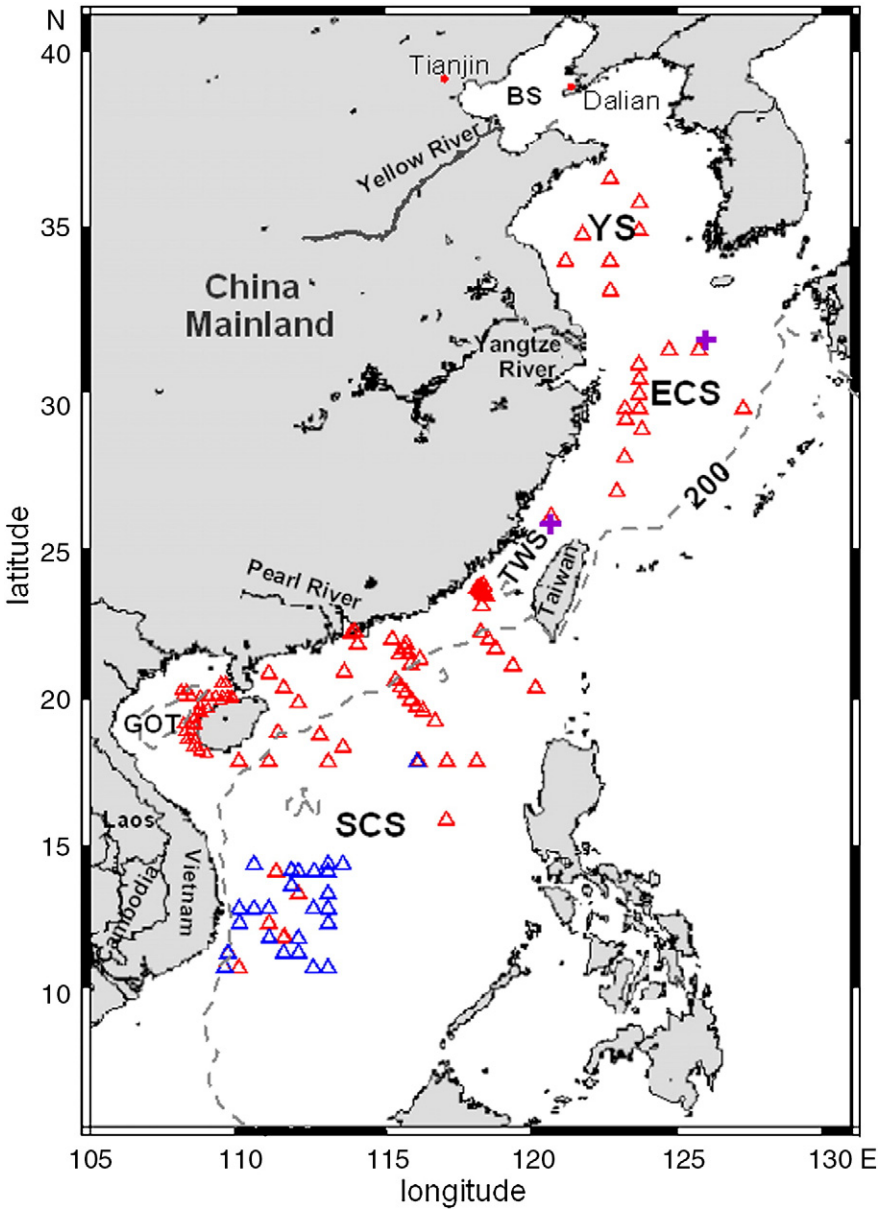

Fig. 1. Map of the study region and location of the field sampling stations. The blue symbols indicate those having both CTD and Profiler II measurements and the purple symbols indicate the two stations for analyzing small scale spatial-temporal variations in Z_{eu} (see text in 3.1); BS: Bohai Sea; YS: Yellow Sea; ECS: East China Sea; TWS: Taiwan Strait; SCS: South China Sea; and GOT: Gulf of Tonkin.

Instruments, Inc.) mounted on a CTD package; PAR profiles were processed with software provided by Biospherical Instruments Inc.

Because these CTD profiles were taken close to the operation ship, the PAR results at sea surface might have been contaminated by ship shadowing or reflected light from the hull. Consequently, the measured PAR(0) might be subject to larger uncertainty. To reduce this measurement-introduced uncertainty, a different approach was used for the derivation of Z_{eu} from the PAR profiles.

Based on Lee et al. (2005, 2007), the vertical variation of PAR(z) can be expressed as:

$$\frac{PAR(z)}{PAR(0)} = \exp(-K_{PAR}(z) \times z) \quad (1)$$

with

$$K_{PAR}(z) = K_1 + \frac{K_2}{(1+z)^{0.5}}. \quad (2)$$

$K_{PAR}(z)$ is the vertical attenuation coefficient of PAR, and K_1 and K_2 are two model constants independent of depth (dependent on the sun angle and the inherent optical properties of the water). As Z_{eu} is the depth that satisfies $K_{PAR}(Z_{eu}) \cdot Z_{eu} = 4.605$, then the values of K_1 and K_2 are required for the derivation of Z_{eu}. Following this guidance, the vertical profile of each PAR measurement is expressed as:

$$\ln(PAR(z)) = \ln(PAR(0)) - \left(K_1 + \frac{K_2}{(1+z)^{0.5}}\right) \times z \quad (3)$$

and values of ln(PAR(0)), K_1 and K_2 for each station were derived by minimizing the difference between Eq. (3) — described profile and the PAR sensor measured profile. In the process, PAR(z) of depths generally deeper than 1 m were used. After K_1 and K_2 are known, Z_{eu} of a specific station can then be calculated algebraically (see Section 2.2).

2.1.3. Comparison between Z_{eu} measured by PAR_{Bios} and by Profiler

To obtain characterization and confidence of the Z_{eu} values derived from the two sensors and measurements, Z_{eu} derived from the PAR_{Bios} (represented as $Z_{eu}(PAR_{Bios})$) and the Z_{eu} derived from hyperspectral Profiler (represented as Z_{eu}(Profiler)) for co-located stations (32 stations, see locations in Fig. 1, the blue symbols) were compared to each other and are presented in Fig. 2. For Z_{eu} in a range of 35–90 m, the average percentage difference between the two sets of Z_{eu} is 7.9%, with a correlation coefficient (R) of 0.942. Such results indicate self-consistency in Z_{eu} from two independent determinations in the field measurements, and provide a first order estimation of uncertainty of *in situ* Z_{eu}. In order to maintain the same standard for assessing MODIS Z_{eu}, and because Z_{eu} values from the Profiler are subject to less uncertainty, for all stations where only Z_{eu} from PAR_{Bios} were available their $Z_{eu}(PAR_{Bios})$ were converted to equivalent Z_{eu}(Profiler) with:

$$Z_{eu}(\text{Profiler}) \approx 1.075\ Z_{eu}(PAR_{Bios}). \quad (4)$$

Therefore, the final *in situ* Z_{eu} data used to assess MODIS Z_{eu} are Z_{eu} from the Profiler (where Profiler data were available) and Z_{eu} derived from Eq. (4) (where only PAR_{Bios} data were available). For simplification, hereafter the Z_{eu} values derived from field measurements are annotated as Z_{eu}^{Mea}; values from the Chl-approach are Z_{eu}^{Chl}; and from the IOP-approach are Z_{eu}^{IOP}.

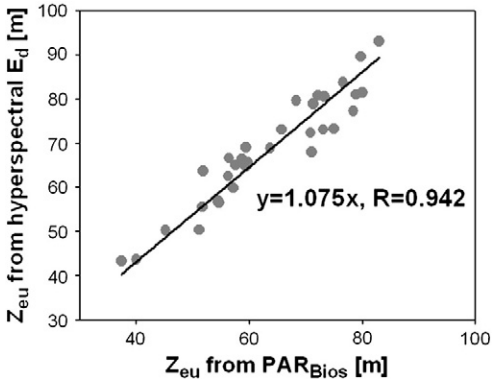

Fig. 2. Z_{eu} derived from PAR_{Bios} versus Z_{eu} derived from hyperspectral E_d.

2.2. Z_{eu} derived from satellite measurements

MODIS daily Level-2 normalized water leaving radiance (nLw) (MODIS/Aqua Reprocessing 1.1) were obtained from the NASA Distributed Active Archive Center and subsequently converted to remote- sensing reflectance (Rrs) via the ratio of nLw to extra-terrestrial solar irradiance (F0) (Gordon, 2005; also see http://oceancolor.gsfc.nasa.gov/forum/oceancolor/). The resolution of these data is approximately 1 km x 1 km at the nadir pixel.

2.2.1. Z_{eu} from empirically derived Chl

This satellite Rrs dataset was used in the OC3M band ratio algorithm (O'Reilly et al., 2000) to calculate Chl. Z_{eu} was subsequently derived by the approach of Morel et al. (2007):

$$\log(Z_{eu}) = 1.524 - 0.436X - 0.0145X^2 + 0.0186X^3 \quad (5)$$

with $X = \log(\text{Chl})$.

2.2.2. Z_{eu} from semi-analytically derived IOPs

The absorption and backscattering coefficients at 490 nm (a(490) and b_b(490)), were derived from the Rrs by applying the Quasi-Analytical Algorithm (Lee et al., 2002, 2007) (also see http://www.ioccg.org/groups/Software_OCA/QAA_v5.pdf for recent updates). K_{PAR}(z) was then calculated (Lee et al., 2005) as a function of a(490) and b_b(490), and the sun angle (θ_a) matching relevant in situ measurements. The IOP-centered Z_{eu} (Lee et al., 2007) was thus derived based on the following equation:

$$K_{PAR}(Z_{eu}) \cdot Z_{eu} = 4.605 \quad (6)$$

The root mean square error in log scale (RMSE) and an averaged percentage error (ε) were then used as measures to evaluate the consistency between the *in situ* and satellite data sets:

$$\varepsilon = \left(\frac{1}{n}\sum_{i=1}^{n}\left|\frac{(Z_{eu}^{IOP})_i - (Z_{eu}^{Mea})_i}{(Z_{eu}^{Mea})_i}\right|\right) \times 100\% \quad (7)$$

$$RMSE = \sqrt{\frac{1}{n}\sum_{i=1}^{n}(\log((Z_{eu}^{IOP})_i) - \log((Z_{eu}^{Mea})_i))^2} \quad (8)$$

RMSE and ε were calculated for Z_{eu}^{Chl} by substituting Z_{eu}^{IOP} with Z_{eu}^{Chl} in Eqs. (7) and (8).

3. Comparison between MODIS Z_{eu} and *in situ* Z_{eu}

3.1. Matching between satellite and in situ measurements

Due to cloud coverage and cost, *in situ* measurements are extremely difficult to obtain with simultaneous measurements between ship surveys and satellite sensors. In order to gain large numbers of matching data points, Bailey et al. (2002) suggest a relaxation in the temporal difference to within ±2–3 h of the satellite overpass. However, temporal mismatch is just one of the factors

affecting the quality of matching between satellite and *in situ* measurements. Another important factor is the spatial mismatch. A satellite sensor (e.g., MODIS) provides a measurement of an averaged property within ~1 km by 1 km, while *in situ* measurements represent an average area of 1 m by 1 m. Consequently, even if the two measurements are carried out simultaneously, data from the two measurements do not "match" each other, unless the observation area is completely homogeneous (i.e., independent of sampling location). This is a more serious source of uncertainty for coastal or near-shore waters where there are greater spatial variations. Because of such inherent mismatches, resulting from measurement strategies, matching-up data between satellite and *in situ* measurements are not always ideal.

In order to obtain an appropriate number of matching observations for meaningful statistical analysis, we relaxed the time-window of overpass to ±48 h. This is based on an evaluation of temporal variations of the research regions and the spatial changes in the 1 km spatial resolution as detailed below.

Short-term variations of Z_{eu} within 13 days were calculated from MODIS Rrs by using the IOP-approach at two field sampling stations (the two purple symbols in Fig. 1) in summer 2004 and 2009 — during cruise surveys (Fig. 3a–b). The 2004 location was at 26.023ºN, 120.486ºW in the Taiwan Strait (TWS), and in 2009 it was at 32.250ºN, 125.750ºW in the East China Sea (ECS). For the Taiwan Strait, the value of Z_{eu} within 13 days was 53±4 m. The mean percentage variation of Z_{eu} within ±2 days (range/mean) was ~13%. For the East China Sea, these numbers were 38±3 m and ~15%, respectively. These temporal variations are comparable to the uncertainty of *in situ* measured Z_{eu}. In addition, Fig. 3c–d presents spatial variations of Z_{eu} around the two stations (extending 1 km to 8 km away from the stations, based on satellite data availability) on August 7, 2004 and August 24, 2009, respectively. The maximum spatial variations of these locations within 8 km distance were ~18% and 33%, respectively. These analyses indicate that no significant extra uncertainties would be introduced from the relaxation of time windows for characterizing MODIS Z_{eu} products.

Following the above data processing method, along with the temporal window for MODIS, a total of 218 match-ups were compiled between *in situ* and satellite Z_{eu} data, which covers a range of 4–93 m. The following characterizes and discusses how satellite Z_{eu} compared with Z_{eu} determined from *in situ* measurements.

3.2. MODIS Z_{eu} compared with in situ Z_{eu}

The comparisons between MODIS Z_{eu} and *in situ* Z_{eu} are presented in Fig. 4. For this dataset, while the non-shelf waters have a Z_{eu} range of 35–93 m, the shelf waters (bathymetry ≤200 m) show quite a wide range of Z_{eu}: 4–75 m. Such an observation indicates that shelf waters are dynamic and complex in biogeochemical contents, and signify different status of ecosystem health.

From satellite estimates, MODIS Z_{eu}^{Chl} shows a high correlation with *in situ* Z_{eu} (R = 0.95), along with a relative difference of 49.9% and an RMSE of 0.205 (Table 1). The bigger relative difference and RMSE values are because MODIS Z_{eu}^{Chl} is apparently (and systematically) higher than *in situ* Z_{eu}; this is also described in Lee et al. (2007) when comparing Z_{eu} with Z_{eu}^{Chl} derived from ship-borne Rrs. In addition to the uncertainties introduced by the mismatches of spatial and temporal scales between *in situ* and satellite measurements, other sources of uncertainty for MODIS Z_{eu}^{Chl} include the empirical estimation of surface Chl and the empirical relationship between Chl and Z_{eu}. Both relationships (Morel et al., 2007; O'Reilly et al., 2000) were developed with data that excluded the China Sea. Fig. 5

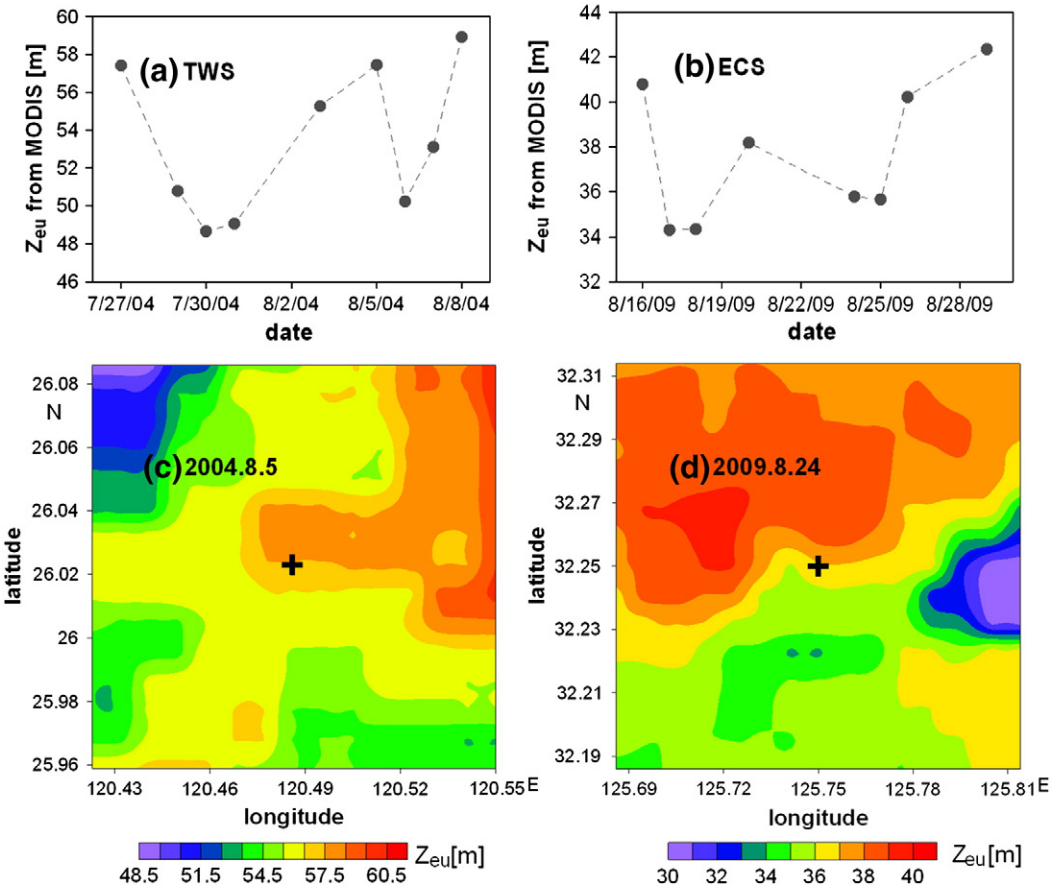

Fig. 3. Temporal and spatial variations of MODIS Z_{eu} at two stations. (a) and (c): TWS (26.023°N, 120.486°E) in July–August 2004; (b) and (d): ECS (32.250°N, 125.750°E) in August 2009.

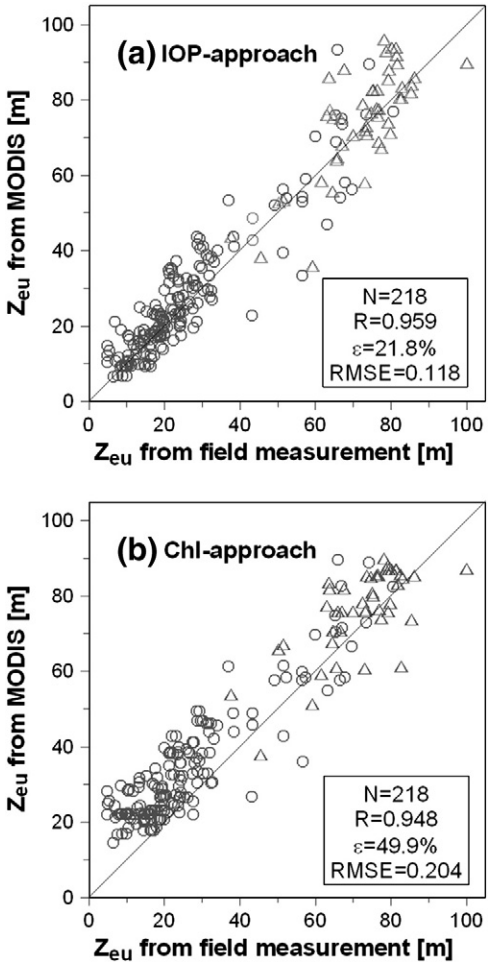

Fig. 4. Comparison between satellite Z_{eu} (by the IOP-approach (a) and Chl-approach (b)) and the Z_{eu} derived from *in situ* measurements. Circles are samples on the shelf (depth ≤200 m) and triangles are those in the basin (depth >200 m); the same applied to the subsequent two figures (Figs. 5–6).

compares Chl estimated by MODIS with Chl from the water samples (Huang et al., 2008; Zhai et al., 2009) (measured flurometrically (Lalli & Parsons, 1993), also with relaxed time-window of satellite overpass to ±48 h). Although the difference is large (RMSE = 0.363), there is no detectable systematic under- or over-estimation of Chl from MODIS for this dataset. The over-estimation of MODIS Z_{eu}^{Chl} apparently resulted from the empirical relationship between Z_{eu} and Chl, as indicated in Fig. 6 where *in situ* Z_{eu} is compared with *in situ* Chl. For the China Sea, at least for this dataset, Z_{eu} would be overestimated if the global empirical model (Morel et al., 2007) was applied (also see comparison of empirical Z_{eu}-Chl relationship in Siegel et al. (2001)). Because the waters studied here are subject to high runoff from major river systems, these results highlight that Z_{eu} of waters with a high suspended sediment load could not be explained well by Chl alone.

For the same dataset (Z_{eu} in a range of 4–93 m from *in situ* measurements), MODIS Z_{eu}^{IOP} also shows a high correlation with *in situ* Z_{eu} (R = 0.96). Compared to Z_{eu}^{Chl}, however, the average relative difference (ε) between MODIS Z_{eu}^{IOP} and *in situ* Z_{eu} is 21.8% (RMSE is 0.118 (Table 1)). Because of extra sources of uncertainty (such as uncertainty in atmosphere correction and/or a mismatch of spatial and temporal scales), the value of ε (and RMSE) between *in situ* Z_{eu} and MODIS Z_{eu}^{IOP} is higher than that obtained between *in situ* Z_{eu} and *in situ* Z_{eu}^{IOP} (Lee et al., 2007). Nevertheless, the results indicate a significantly improved estimation of Z_{eu} from MODIS with the IOP-approach, and consequently improvements of estimation of primary production where the Z_{eu} product is required (Behrenfeld & Falkowski, 1997a; Shang et al., 2010). This result is even more exciting because most (78%) of the dataset were measured on the shelf, and the composition of shelf water constituents are generally complex and dynamic. Such an improvement on the satellite Z_{eu} estimation may be attributed to the fact that there is no dependence on Case-1 assumptions when applying the IOP-approach. Meanwhile, the discrepancy between MODIS Z_{eu} and *in situ* Z_{eu} shown above suggests an upper limit of Z_{eu} uncertainty from MODIS since there are extra sources of uncertainty in satellite remote sensing, while the results in Lee et al. (2007) indicated a lower limit of uncertainty, when the IOP-approach is applied.

Note that the RMSE value is 0.363 and the average relative difference is ~69% when *in situ* Chl was compared with the match-up satellite Chl (see Fig. 5). Our results indicate that, at least for waters in the China Sea, MODIS-derived Z_{eu}^{Chl} (Fig. 4, right) has better accuracy than MODIS-derived Chl. This is in part because euphotic zone depth is an optical property, while chlorophyll-a concentration is a biological property. When they are derived from a remote sensing reflectance, the former has no dependence on the concentration-normalized optical properties (e.g., chlorophyll-specific absorption coefficient), while the latter does (explicitly or inexplicitly). MODIS-derived Z_{eu}^{IOP}, however, has much higher accuracy (a factor of 3 smaller RMSE and relative difference) than MODIS-derived Chl.

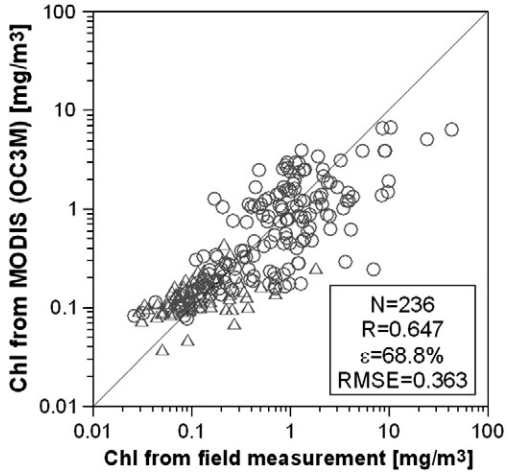

Fig. 5. Comparison between Chl derived from MODIS and Chl from surface water samples.

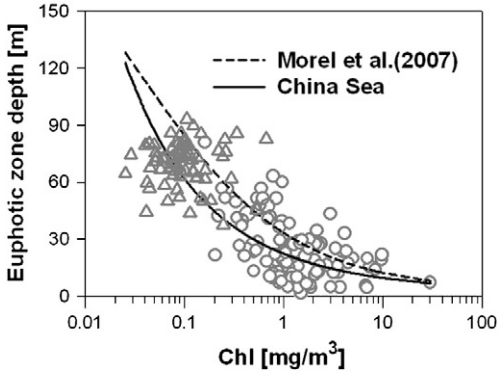

Fig. 6. Relationship between *in situ* Z_{eu} and *in situ* Chl, with all data from the China Sea. The empirical, global, relationship developed by Morel et al. (2007) is superimposed on the figure (dashed line). The local empirical relationship (solid line) for this dataset is: $\log_{10}(Z_{eu}) = 1.35 - 0.4026\,X + 0.0375\,X^2, X = \log_{10}(\mathrm{Chl}), R = 0.767, N = 190$.

Table 1
Error statistics for the comparison between the Z_{eu} derived from *in situ* measurements and from MODIS Rrs.

	IOP-approach		Chl-approach		N
	ε(%)	RMSE	ε(%)	RMSE	
TWS	18.5	0.091	37.3	0.157	56
GOT	37.6	0.171	107.9	0.331	43
SCS	15.9	0.103	34.5	0.165	80
YS and ECS	21.3	0.107	35.7	0.148	39
Shelf water	25.1	0.130	60.6	0.229	170
Basin water	10.2	0.060	12.2	0.062	48
Total	21.8	0.118	49.9	0.205	218

Especially, the IOP-approach is *not* a regression analysis to develop empirical relationships (and coefficients), but rather an *independent* test/evaluation of algorithms that were developed earlier. Such efforts provide users more insights of performances and characterizations of independently developed algorithms in a broad range of environments. Furthermore, a product with low RMSE adds confidence in applying MODIS products for monitoring water clarity and/or ecosystem health.

4. Distribution and variation of MODIS Z_{eu} in the China Sea

We then used the IOP-approach to derive a climatological seasonal mean Z_{eu} for the China Sea (see Fig. 7) from the monthly mean MODIS Rrs for the time frame of December 2002 through November 2009. The results presented hereafter are limited to the region west of the dashed black line in Fig. 7.

In general, Z_{eu} is deep (maximum ~110 m) in the oligotrophic South China Sea (SCS, ~5000 m at maximum depth (Liu et al., 2002)) when compared to Z_{eu} in the complex and relatively eutrophic East China Sea (ECS) (Gong et al., 2003). This is because the ECS has a wide continental shelf and is associated with freshwater discharge from the Yangtze River (the third largest river in the world). There is a distinct tongue of low Z_{eu} water out of the Yangtze River estuary. The value of Z_{eu} within this tongue is extremely low in winter (~<10 m overlaid on the ECS background level of ~40 m). The tongue of low Z_{eu} reaches further offshore in winter, a dry season when the river discharge is low (minimum ~30 km^3/month, mean value for 1950–1990, (Xu & Milliman, 2009)), while it shrinks in summer. This suggests that sediment resuspension (driven by strong winds in winter) (Song et al., 2006) has a higher impact on the shallowing of Z_{eu} in this region — when compared to the river outflow (Xu & Milliman, 2009).

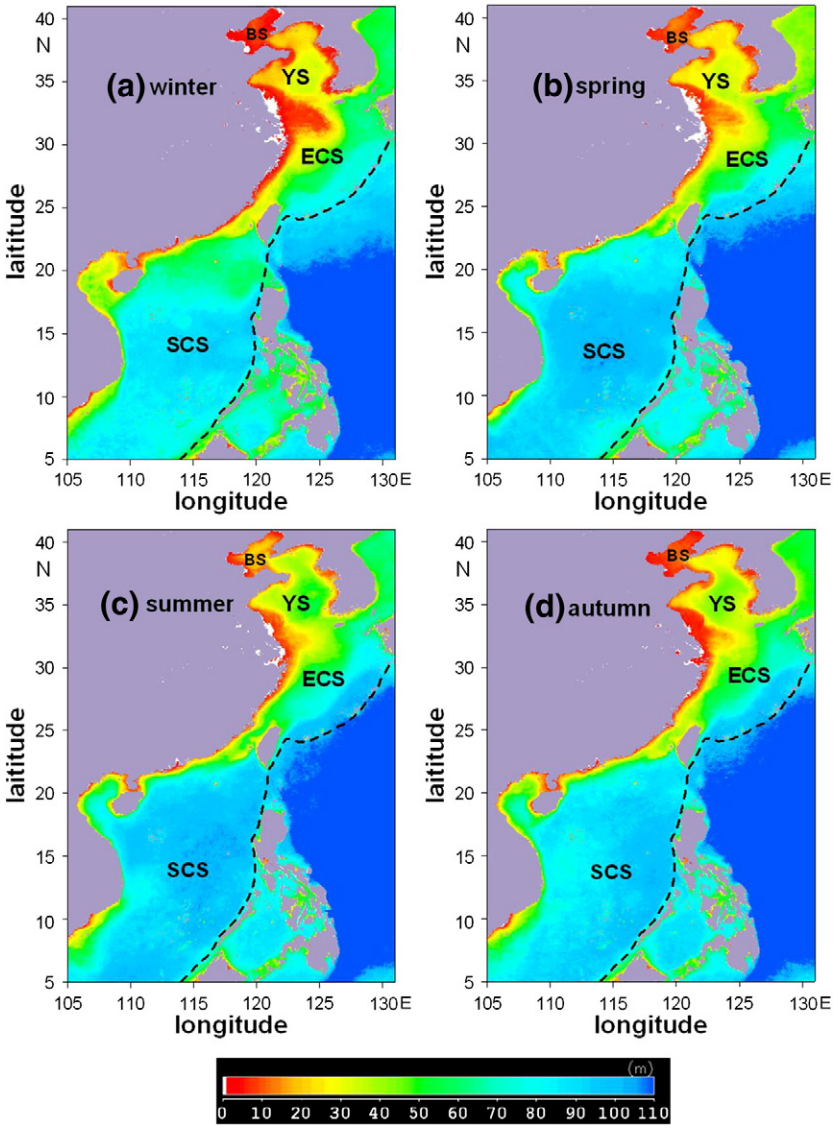

Fig. 7. Climatological seasonal mean Z_{eu} in the China Sea (IOP-approach, 2002–2009).

In the SCS, winter is the season with the highest primary production in the surface layer, which is attributed to nutrient pumping from deep water, which is in turn induced by strong wind mixing (Chen, 2005). Consequently, Z_{eu} is shallower in winter (~85 m) when compared to other seasons (~110 m) for the SCS. On the other hand, because of the intrusion of the oligotrophic Kuroshio and Taiwan Warm Current to the ECS (driven by southerly winds) (Lee & Chao, 2003), Z_{eu} is generally deeper in summer in the ECS, although primary productivity in some areas is three times higher in summer than that in other seasons (Gong et al., 2003).

In addition, the Bohai Sea is an area of notably shallow Z_{eu} (~6 m in winter, ~9 m in spring, ~8 m in autumn, and ~14 m in summer). Considering that the Bohai Sea is a semi-enclosed shallow sea (average water depth is ~18 m) surrounded by several big cities (e.g., Tianjin and Dalian), and that the Yellow River (the sixth longest river in the world) empties into this marine system, this character is quite reasonable and expected.

5. Conclusions

For the first time, the quality of the two MODIS Z_{eu} products is characterized with extensive field-measured Z_{eu} in the China Sea, a marginal sea that features one of the widest continental shelves in the world and has an input from the two large rivers. Three main results are found from this study. First, MODIS Z_{eu} products in the China Sea are robust, even in shelf waters ($\leq$200 m). Second, Z_{eu} produced with the IOP-approach (which has no dependence on Case-1 assumptions) is more reliable than those produced with empirically derived Chl (which is dependent on Case-1 assumptions). And third, Z_{eu} is generally shallower in winter in the China Sea (when compared to summer), and is shallower in the East China Sea than in the South China Sea.

Results shown here provide the research and monitoring communities an increased confidence when applying the satellite Z_{eu} products (especially those produced with the IOP-approach) to the primary production estimates and environmental change research — both at the local and global scales.

Acknowledgements

This work was supported jointly by the High-Tech R&D Program of China (#2006AA09A302 & 2008AA09Z108), the National Basic Research Program of China (#2009CB421200 & 2009CB421201), NSF of China (#40821063) and the China Scholarship Council. Supports provided by NASA's Water- and Energy Cycle Program (Lee) are greatly appreciated. We thank Drs. H. Hong, M. Dai, H. Gao, Y. Li, J. Hu, B. Huang, J. Sun, W. Zhai, Z. Liu and L. Huang for providing *in situ* measured PAR and Chl data. We thank the Ocean Biology Processing Group (OBPG) at the Goddard Space Flight Center for generation and distribution of the MODIS products.

References

Bailey, S. W., McCLain, C. R., Werdell, P. J., & Schieber, B. D. (2002). Normalized water-leaving radiance and chlorophyll-a match-up analyses. In S. B. Hooker, & E. R. Firestone (Eds.), *NASA Technical. Memorandum. 2000-206892 SeaWiFS postlaunch calibration and validation analyses, part 2, 10* (pp. 45—52). Greenbelt, Maryland: NASA Goddard Space Flight Center.

Bailey, S. W., & Werdell, P. J. (2006). A multi-sensor approach for the on-orbit validation of ocean color satellite data products. *Remote Sensing of Environment*, *102*, 12—23.

Behrenfeld, M. J., & Falkowski, P. G. (1997a). A consumer's guide to phytoplankton primary productivity models. *Limnology and Oceanography*, *42*(7), 1479—1491.

Behrenfeld, M. J., & Falkowski, P. G. (1997b). Photosynthetic rates derived from satellite-based chlorophyll concentration. *Limnology and Oceanography*, *42*(1), 1—20.

Buesseler, K. O., Lamborg, C. H., Boyd, P. W., Lam, P. J., Trull, T. W., Bidigare, R. R., Bishop, J. K. B., Casciotti, K. L., Dehairs, F., Elskens, M., Honda, M., Karl, D. M., Siegel, D. A., Silver, M. W., Steinberg, D. K., Valdes, J., Mooy, B. V., & Wilson, S. (2007). Revisiting carbon flux through the ocean's twilight zone. *Science*, *316*(5824), 567—570. doi:10.1126/science.1137959

Chen, Y. l. L. (2005). Spatial and seasonal variations of nitrate-based new production and primary production in the South China Sea. *Deep-Sea Research I*, *52*, 319—340.

Darecki, M., & Stramski, D. (2004). An evaluation of MODIS and SeaWIFS bio-optical algorithms in the Baltic Sea. *Remote Sensing of Environment*, *89*, 326—350.

Gong, G., Wen, Y., Wang, B., & Liu, G. (2003). Seasonal variation of chlorophyll a concentration, primary production and environmental conditions in the subtropical East China Sea. *Deep-Sea Research II*, *50*, 1219—1236.

Gordon, H. R. (2005). Normalized water-leaving radiance: Revisiting the influence of surface roughness. *Applied Optics*, *44*, 241—248.

Gordon, H. R., & Morel, A. (1983). *Remote assessment of ocean color for interpretation of satellite visible imagery: A review.* New York: Springer-Verlag.

Huang, B. Q., Lan, W. L., Cao, Z. R., Dai, M. H., Huang, L. F., Jiao, N. Z., & Hong, H. S. (2008). Spatial and temporal distribution of nanoflagellates in the northern South China Sea. *Hydrobiologia*, *605*, 143—157.

IOCCG (2006). Remote sensing of inherent optical properties: Fundamentals, tests of algorithms, and applications. In Z. -P. Lee (Ed.), *Reports of the international ocean-colour coordinating group*, *Vol. 5*, Dartmouth, Canada: IOCCG.

Kirk, J. T. O. (1994). *Light and photosynthesis in aquatic ecosystems.* New York: Cambridge University Press.

Lalli, C. M., & Parsons, T. R. (1993). *Biological oceanography: An introduction.* Oxford: Butterworth-Heinemann Ltd.

Lee, Z., Carder, K. L., & Arnone, R. A. (2002). Deriving inherent optical properties from water color:a multiband quasi-analytical algorithm for optically deep waters. *Applied Optics*, *41*(27), 5755—5772.

Lee, H., & Chao, S. (2003). A climatological description of circulation in and around the East China Sea. *Deep-Sea Research II*, *50*, 1065—1084.

Lee, Z., Du, K., Arnone, R., Liew, S., & Penta, B. (2005). Penetration of solar radiation in the upper ocean: A numerical model for oceanic and coastal waters. *Journal of Geophysical Research*, *110*, C09019.

Lee, Z. P., Weidemann, A., Kindle, J., Arnone, R., Carder, K. L., & Davis, C. (2007). Euphotic zone depth: Its derivation and implication to ocean-color remote sensing. *Journal of Geophysical Research*, *112*, C03009. doi:10.1029/2006JC003802

Liu, K. K., Chao, S. Y., Shaw, P. T., Gong, G. C., Chen, C. C., & Tang, T. Y. (2002). Monsoon-forced chlorophyll distribution and primary production in the South China Sea: Observations and a numerical study. *Deep-Sea Research I*, *49*, 1387—1412.

Melin, F., Zibordi, G., & Berthon, J. E. (2007). Assessment of satellite ocean color products at a coastal site. *Remote Sensing of Environment*, *110*(2), 192—215.

Morel, A., & Gentili, B. (2004). Radiation transport within oceanic (case 1) water. *Journal of Geophysical Research*, *109*, C06008.

Morel, A., Huot, Y., Gentili, B., Werdell, P. J., Hooker, S. B., & Franz, B. A. (2007). Examining the consistency of products derived from various ocean color sensors in open ocean (Case 1) waters in the perspective of a multi-sensor approach. *Remote Sensing of Environment*, *111*, 69—88.

O'Reilly, J. E., Maritorena, S., Siegel, D., O'Brien, M. C., Toole, D., Mitchell, B. G., Kahru, M., Chavez, F. P., Strutton, P., Cota, G. F., Hooker, S. B., McClain, C. R., Carder, K. L., Muller-Karger, F., Harding, L., Magnuson, A., Phinney, D., Moore, G. F., Aiken, J., Arrigo, K. R., Letelier, R., & Culver, M. (2000). Seawifs postlaunch calibration and validation analyses, part 3. In S. B. Hooker, & E. R. Firestone (Eds.), *NASA technical memorandum*. Greenbelt, Maryland: NASA Goddard Space Flight Center.

Platt, T., & Sathyendranath, S. (1988). Oceanic primary production: Estimation by remote sensing at local and regional scales. *Science*, *241*(4873), 1613—1620.

Preisendorfer, R. W. (1986). Secchi disk science: Visual optics of natural waters. *Limnology and Oceanography*, *31*(5), 909—926.

Sathyendranath, S., Gouveia, A. D., Shetye, S. R., Ravindran, P., & Platt, T. (1991). Biological control of surface temperature in the Arabian Sea. *Nature*, *349*, 54—56.

Shang, S. L., Behrenfeld, M. J., Lee, Z. P., O'Malley, R. T., Wei, G. M., Li, Y. H., & Westberry, T. (2010). *Comparison of primary productivity models in the Southern Ocean-preliminary results. Prodeedings of SPIE, 7678.*

Siegel, D. A., Westberry, T. K., O'Brien, M. C., Nelson, N. B., Michaels, A. F., Morrison, J. R., Scott, A., Caporelli, E. A., Sorensen, J. C., Maritorena, S., Garver, S. A., Brody, E. A., Ubante, J., & Hammer, M. A. (2001). Bio-optical modeling of primary production on regional scales: The Bermuda BioOptics project. *Deep-Sea Research II*, *48*, 1865—1896.

Song, Z. J., Huang, H. J., Du, T. Q., Liu, F., & Ni, J. L. (2006). Suspended sediment near radial sand ridge area in the south Yellow Sea. *Marine Geology and Quaternary Geology*, *26*(6), 19—25.

Takahashi, T., Sutherland, S. C., Sweeney, C., Poisson, A., Metzl, N., Tilbrook, B., Bates, N., Wanninkhof, R., Feelyf, R., Sabine, C., Olafsson, J., & Nojiri, Y. (2002). Global sea–air CO_2 flux based on climatological surface ocean pCO_2, and seasonal biological and temperature effects. *Deep Sea Research II*, *49*, 1601—1622.

Tyler, J. E. (1968). The Secchi disc. *Limnology and Oceanography*, *13*(1), 1—6.

Xu, K., & Milliman, J. D. (2009). Seasonal variations of sediment discharge from the Yangtze River before and after impoundment of the Three Gorges Dam. *Geomorphology*, *104*, 276—283.

Zhai, W., Dai, M., & Cai, W. (2009). Coupling of surface pCO2 and dissolved oxygen in the northern South China Sea: Impacts of contrasting coastal processes. *Biogeosciences*, *6*, 2589—2598.

Zhang, C. Y., Hu, C., Shang, S., Müller-Karger, F. E., Li, Y., Dai, M. H., Huang, B. Q., Ning, X. R., & Hong, H. S. (2006). Bridging between SeaWiFS and MODIS for continuity of chlorophyll-a concentration assessments off Southeastern China. *Remote Sensing of Environment*, *102*, 250—263.